HIGH-FREQUENCY ULTRASONIC TRANSDUCERS Fabrication, Characterisation, Performance

Franck Levassort, Louis-Pascal Tran-Huu-Hue, Jean-Marc Grégoire, Marc Lethiecq

HIGH-FREQUENCY ULTRASONIC TRANSDUCERS
Fabrication, Characterisation, Performance

Franck LEVASSORT, Louis-Pascal TRAN-HUU-HUE,
Jean-Marc GREGOIRE, Marc LETHIECQ

GIP ULTRASONS / LUSSI - CNRS FRE 2448
François Rabelais University – Tours, FRANCE

Introduction
High-frequency ultrasound devices have been developing in many fields such as electronic filters and resonators, material characterisation (acoustic microscopes), non-destructive testing and medical diagnostics. This paper will deal with ultrasonic transducers which are designed for imaging applications, particularly for medical diagnosis in organs such as skin, eye and blood vessels, as well as for non-destructive evaluation and small animal examinations. This field has generated a great deal of research as well as commercial products, attested by many publications in both specialised and general scientific journal [1-4]. The frequency range starts around 20 MHz, and extends up to 100 MHz.

I. General transducer requirements
I.1. Electroacoustic requirements
The classical single-element transducer is composed of a piezoelectric plate or disc poled along the thickness direction, whose thickness defines the resonance frequency of the device (Figure 1). The piezoelectric element (typically a ferroelectric ceramic), has an acoustic impedance (*i.e.* around 33 MRa) much higher than biological tissues (close to that of water, *i.e.* 1.5 MRa). This large difference leads to poor acoustic matching and low axial resolution.
Consequently, other layers are added to this active layer. First, on its rear face, a thick layer is bonded (backing) [5]. It serves as a mechanical support for the active element, but acoustic energy flows by the rear face. The closer the backing acoustic impedance is to that of the active layer, the more energy is lost. The consequence is a lower sensitivity but a higher axial resolution. The attenuation coefficient and the thickness of the backing layer must be sufficient so that no energy can be radiated back to the active layer, because this would produce parasitic echoes.
Secondly, on the front (*i.e.* between the piezoceramic and the propagation medium), a matching layer is used. Its design is optimised in order to increase the energy transfer from the active layer to the tissues [6, 7]. The thickness of this matching layer is generally around a quarter-wavelength at the resonance frequency, and its acoustic impedance is intermediate between those of the piezoceramic and tissues. The use of a matching layer thus improves the sensitivity of the transducer. Moreover, since the acoustic energy can better flow towards the tissues, the duration of acoustic resonance in the active layer is decreased. Consequently, the matching layer also improves axial resolution. Influence of these two elements on the impulse and frequency responses transducers is shown in Figure 1 and a trade-off has to be found for each application. The active layer is typically a PZT-based material, while matching layers and backings are polymer-based.

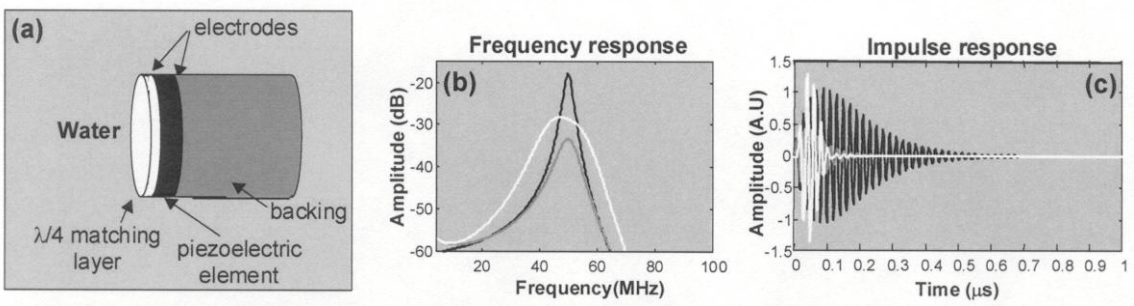

Figure 1 : (a) Classical diagram of a single-element transducer. (b) and (c) Frequency and impulse responses of : black line : piezoelectric element (water on front face and air on rear face), grey line : piezoelectric element+backing, white line : with matching layer.

I.2. Radiation pattern requirements

The radiation pattern of a focused single-element transducer is defined by the size of the active element (D) and the focal distance (F) (Figure 2). In the case where a lens is used for focusing, (F) can be deduced from the lens curvature (R_c) and the sound wave velocities in the lens and propagation media (Figure 3).

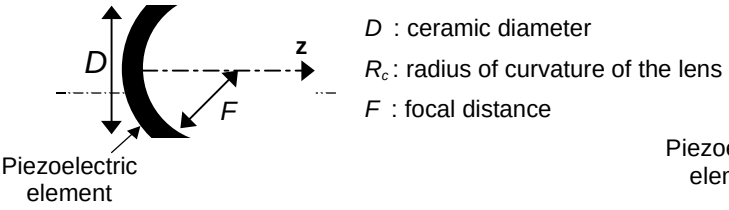

Figure 2 : Shape-focused transducer.

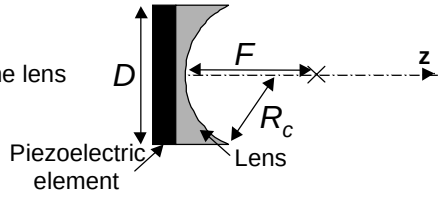

Figure 3 : Lens-focused transducer.

Lateral resolution is linked to the width of the acoustic beam and is optimum at the focal distance. Approximate expressions of this lateral resolution ($R_{lateral}$), depth of field (DOF) and axial resolution (R_{axial}) for a spherical shape transducer are defined (eq. 1). The ratio between the focal distance and the diameter of the piezoelectric element, called the f-number ($f_{\#}$), allows to define the trade-off between lateral resolution and depth of field. λ is the wavelength at nominal frequency and BWR_{-6dB} is the relative bandwidth at –6 dB.

$$f_{\#} = \frac{F}{D}, \qquad R_{lateral} \approx \lambda \times f_{\#}, \qquad DOF \approx 7\lambda \times f_{\#}^2, \qquad R_{axial} \approx \frac{\lambda}{2BWR_{-6dB}} \quad (1)$$

The resolutions and depth of field can change of several orders of magnitude according to frequency. High frequencies lead to high resolutions but, due to increase of attenuation in tissues, the depth of penetration in the explored medium is reduced. The acoustic properties of the explored medium as well as of the driving electronics also influence the imaging performance [4, 8].

1.3. Typical size

For typical fixed values for medical imaging as the centre frequency at 50 MHz (i.e. a f-number of 2.5, a focal distance at 7.5 mm, a relative bandwidth (-6dB) at 60%), the corresponding diameter D is at 3 mm, the thickness of the piezoelectric element (ceramic) is around 45 μm, the axial and lateral resolutions are respectively around 30 and 75 μm, and the depth of field around 1.3 mm. These resolutions correspond to those generally required for skin imaging.

II. Piezoelectric materials

II.1. General requirements

For the piezoelectric material, in particular for medical applications, two of the most important material parameters are the effective electromechanical coupling coefficient k_{eff} of the main vibration mode used and the acoustic impedance Z.

The k_{eff} factor represents the piezoelectric activity of the material in the considered mode of vibration, in other words the capability of the material to convert electrical energy into acoustic energy (or vice-versa) in a short time; it should of course be as high as possible. This factor depends not only on the material properties but also on the geometry of the active element. In medical imaging applications, all vibration modes are longitudinal, *i.e.* the displacements are in the poling direction which defines the thickness dimension. For large plates or discs (thickness much lower than lateral dimensions), the thickness coupling factor k_t is used. For bars or pillars (thickness higher than lateral dimensions), the factor is k_{33}. For the intermediate case of an array element (one small and one large lateral dimensions with a thickness value between them), k'_{33} factor is defined [9]. The value of the dielectric constant also has an important role on the electrical matching.

Figure 4 represents values of the thickness mode coupling factor (k_t) versus the acoustic impedance (Z) for a wide range of available piezoelectric materials. It can be observed that no material allows to obtain both high coupling and low acoustic impedance (ideal area in Figure 4). The best trade-off must be found among these materials. For almost all medical transducers applications, PZT piezoceramics are used because of their high coupling factor, even if their acoustic impedance is high, since this can be compensated for by using acoustic matching layers in the transducer structure. For a given application, properties such as dielectric constant and grain size allow to choose a specific material reference. A large range of properties can be found from relatively low (a few hundred) to very high (a few thousand) relative dielectric constants with grain sizes from one to ten micrometers. For large area devices such as single element transducer, a moderate dielectric constant allows good electrical matching to cables and electronics (which are typically at 50 to 80 ohms) (area 1), while array elements require much higher dielectric constants (area 2).

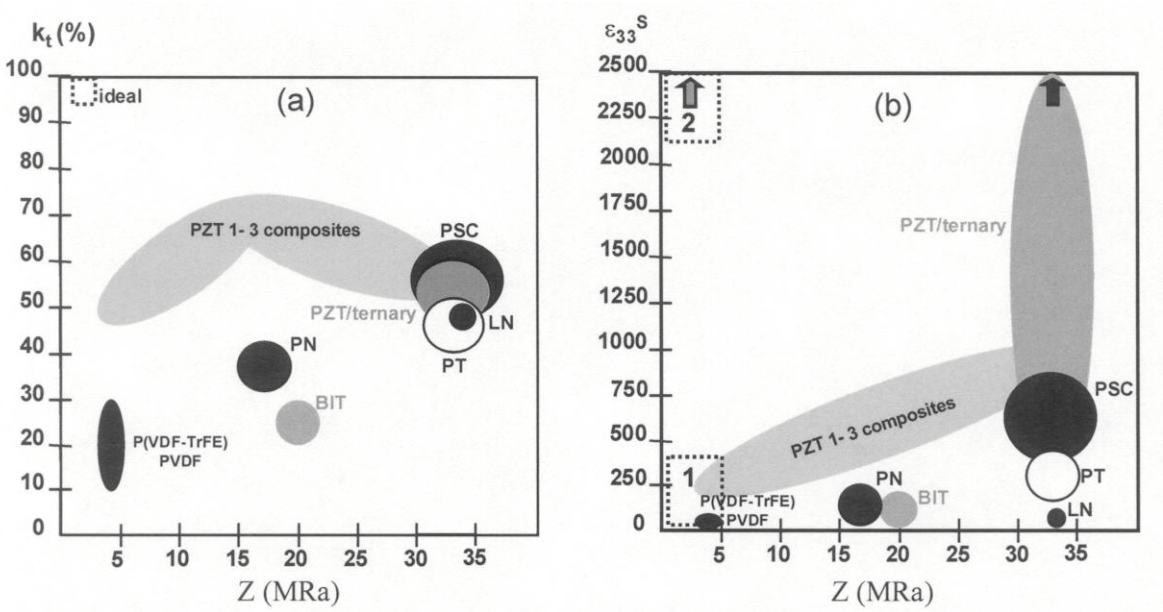

PZT: Lead zirconate titanate, **PT**: Lead titanate, **PN** : Lead metaniobate, **PVDF** : Polymer, **P(VDF-TrFE)** : Copolymer, **BIT** : Bismuth titanate, **PSC** : Piezoelectric single crystals, **LN** : Lithium Niobate, **1-3 composites** : PZT and polymer

Figure 4 : (a) Electromechanical coupling factor in thickness mode (k_t). (b) Relative dielectric constant at constant strain (ε_{33r}^S) versus of the acoustic impedance (Z) for a wide range of piezoelectric materials.

II.2. Characterisation

Measurements of the complex electrical impedance as a function of frequency of the piezoelectric materials allow, with an equivalent electrical scheme [10], to obtain dielectric, mechanical and electromechanical properties by a fitting process. In some cases, standards on piezoelectricity [9, 11] can be used: the experimental curves are then exploited directly using simple formulas.

The standard set-up is composed of a network analyser with its impedance test kit and a spring clip fixture to make electrical contacts with the electroded piezoelectric material (Figure 5(a)). These contacts have a great importance in particular at high frequency, since to stay in free resonator condition, their sizes must be very small in comparison with the size of the measured sample and the forces applied must not perturbate the resonance mode. Moreover, the quality of the contact is very important to avoid a too large contact impedance.

Figure 5(b) shows the typical resonance of a PZT disk made by tape-casting which has an antiresonant frequency around 50 MHz. At high frequency, the piezoelectric element is often deposited on a substrate during the fabrication process (Figure 5(a)) and the experimental electrical impedance depends on this substrate. With an electrical equivalent circuit, such as KLM which is well adapted to multilayer structures (electrodes, piezoelectric layer and substrate), and knowing all the acoustic properties of electrodes and substrate, the fitting process allows to obtain the properties of the piezoelectric layer (Figure 4 (c))[12, 13].

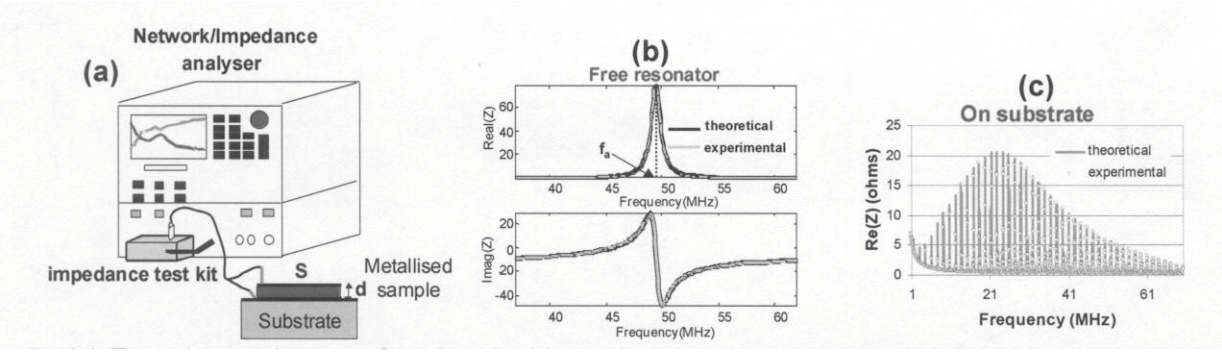

Figure 5 : (a) Experimental set-up for electrical impedance measurements. (b) Experimental and theoretical complex impedance (fit) of high frequency piezoelectric disk in free resonator conditions. (c) Experimental and theoretical impedance (real part) (fit) of high frequency piezoelectric thick film on alumina substrate.

Typical parameters characterised are the following:

- Resonant (f_r) and antiresonant (f_a) frequencies which correspond respectively to maximum of real admittance and real impedance;
- The thickness coupling factor (vibration corresponding to a thickness mode) can be calculated with $k_t = \sqrt{\frac{\pi}{2}\frac{f_r}{f_a}\cot\left(\frac{\pi}{2}\frac{f_r}{f_a}\right)}$ (2);
- The longitudinal wave velocity $v = 2df_a$ (d: thickness of the piezoelectric sample) (3);
- Dielectric constant ε is obtain from the capacitance C_0 after resonance and dimensions;
- Mechanical quality factor (or mechanical losses δ_m) $Q_m = \frac{f_a}{\Delta f}$ (4) where Δf corresponds to the frequency width at half the maximum resistance;
- Dielectric losses appear as an offset on resistance curves, the measurement can be made at twice the anti-resonant frequency and they can change with frequency.

Several authors [14-16] have proposed specific measurement methods to obtain high-frequency properties of piezoelectric materials.

II.3. Polymers/Copolymers

Piezopolymers such as PVDF or copolymers [17, 18] can be purchased as films with thickness of one to a few tens of microns which can be directly used for high frequency applications. Their coupling factors are relatively low (between 15 and 30%) and relative clamped dielectric constant is low (around 5). These two last properties tend to give a relatively low sensitivity and the electric matching is difficult. But their acoustic impedance is low and close to that of tissues (between 4 and 5 MRa), so acoustic matching is not indispensable (Table 1).

Table 1 : Main properties of a P(VDF-TrFE) piezoelectric copolymer film.

material	$\varepsilon_{33}^S/\varepsilon_0$	v_l (m/s)	k_t (%)	δ_e (%)	δ_m (%)	Z (MRa)	ref
P(VDF-TrFE)	4.1	2380	29	6.9	4.0	4.6	[19]

$\varepsilon_{33}^S/\varepsilon_0$: clamped dielectric constant; v_l: longitudinal wave velocity; k_t: thickness coupling factor; δ_e: dielectric losses; δ_m: mechanical losses; **Z**: acoustic impedance.

The second main and determinant advantage is that the flexibility of the film allows a direct focusing and avoids the addition of a lens (Figure 6).

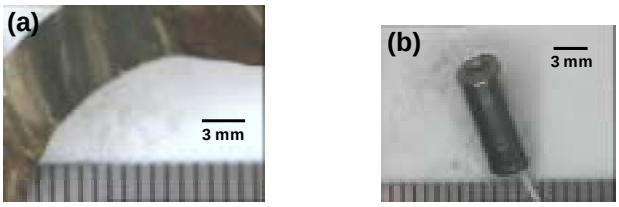

Figure 6 : (a) Copolymer sheet. (b) High frequency copolymer based transducer.

Even with a relatively low (k_t), these materials are widely used for high frequency transducer fabrication in the range of from 20 MHz to over 100 MHz.

II.4. Ceramic thick films

Many processes are possible and have been developed [20] such as screen-printing, tape-casting, spin or dip coating processes and spray techniques [21-24] to make piezoelectric thick films (few tens of microns). The three first ones are widely used techniques, in particular for imaging applications. In each case, the samples (generally circular shape) are made directly in final shape and avoid machining, namely lapping, which can represent a critical step where micro-cracks or breakdown can appear. The tapes can be used to manufacture thin self-supported disks as shown on Figure 7.

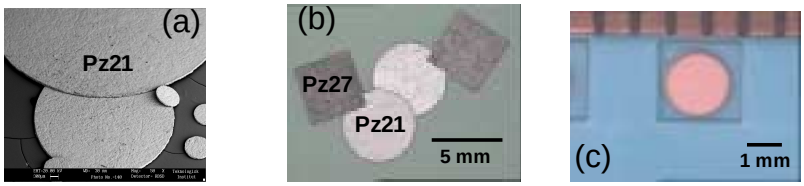

Figure 7 : Tape-casted self supported disk photographs. (a) (b) from Ferroperm piezoceramics (Denmark), (c) from Laboratoire de Céramique (EPFL, Switzerland).

Table 2 summarises several representative characteristics of self-supported samples where properties are slightly lower than those of bulk ceramics (in particular k_t) but their actual performance allow to integrate these elements in transducers which deliver satisfying properties.

Table 2 : Properties of self supporting samples made by tape-casting.

Materials	$\varepsilon_{33}^S/\varepsilon_0$	k_t (%)	f_a (MHz)	ρ (kg/m^3)	δ_m (%)	**ref**
Pz21 (PNNZT)	1920	43	33.9	7420	4.7	[25]
Pz29 (PZT)	1035	35.5	34.1	6900	6.0	[25]
PZT	675	43	46	-	3.6	[26]

$\varepsilon_{33}^S/\varepsilon_0$: clamped dielectric constant; k_t: thickness coupling factor;
f_a : antiresonant frequency; ρ: density; δ_m: mechanical losses.

The substrates used for the deposited thick films can be used in two ways. First, the substrate can be chosen to be used directly as a backing for the transducer [27]. Many conditions are necessary for this in terms of sintering temperature (for the thick films) and acoustic properties for the transducer. Porous PZT can be a good choice (Figure 8(a)). This method leads to an integrated device. Secondly, the substrate can be chosen only as an intermediate material. For example, The PZT thick film is deposited on an aluminium substrate (Figure 8(b)) [28]. On the other side, epoxy resin loaded with Ag powder is added as the future backing. Finally, the Al substrate is etched and a new electrode is deposited on the front face of the thick film. This method allows to optimise the choice of these two materials for the future transducer.

For these two cases, properties of the piezoelectric thick films are given in Table 3 where the performance obtained can be relatively high, but the reproducibility remains an important problem to be solved. Moreover, the choice of the bottom electrode material and thickness can also greatly influence the final properties.

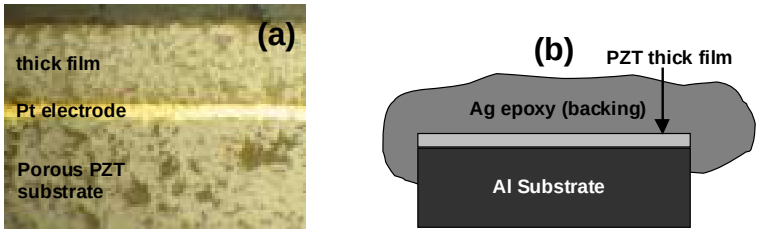

Figure 8 : (a) Cross section of optical microscope photograph of screen-printed PZT thick film on porous PZT substrate. (b) Schematic screen-printing process with intermediate substrate.

Table 3 : Properties of screen-printed samples on different substrates.

material	process	substrate	e (μm)	$\varepsilon_{33}^S/\varepsilon_0$	v_l (m/s)	k_t (%)	δ_e (%)	δ_m (%)	Z (MRa)	ref
PZT/PGO	Screen-printing	PZT	35.5	334	3240	47	4.7	4.8	-	[27]
PZT/PGO	Screen-printing	Al_2O_3	39	342	3940	39.7	2.0	1.5	-	[27]
PZT	Spin coating	Al	20	220	3950	24.4	-	-	21.8	[28]

$\varepsilon_{33}^S/\varepsilon_0$: clamped dielectric constant; v_l: longitudinal wave velocity; k_t: thickness coupling factor; δ_e: dielectric losses; δ_m: mechanical losses; Z: acoustic impedance.

II.5. Composites

In combining a high coupling piezoceramic (such as a soft PZT) and a low acoustic impedance polymer, it is possible to obtain simultaneously the two essential requirements as mentioned in section II.1. Different spatial arrangements (described by the connectivity [29]) between the two phases are possible and influence directly the homogenised material performance. For high frequency applications, 1-3, 2-2 and 0-3 piezo-composites have been investigated. The 1-3 connectivity is of great interest and delivers high performance (Figure 9(a)). This connectivity corresponds to ceramic pillars in a polymer matrix. For example, with a ceramic volume fraction around 40%, the value obtained for k_t is higher than that of the ceramic alone (Figure 9(b)).

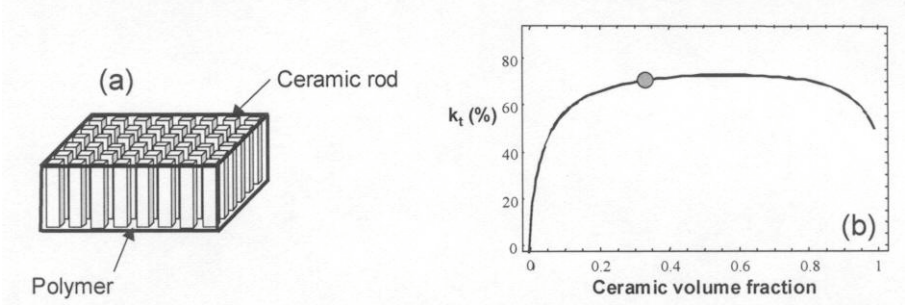

Figure 9 : (a) Schematic representation of a 1-3 piezo-composite sample. (b) Typical variation of the thickness coupling factor (k_t) of a 1-3 piezo-composite as a function of the volume fraction of the ceramic.

The most common process for 1-3 piezo-composite fabrication is the “dice and fill” technique which appeared at the beginning of the 80’s [30]. Other methods such as lost mould, fused deposition, injection-moulding techniques have been widely used [31-33]. At high frequency, the spatial scale for all these methods (i.e. periodicity) limits the good vibration in thickness mode generally around 25 MHz. Alternative method is to develop ceramic fibres which are aligned in random positions and embedded in a polymer matrix as a 1-3 composite [34, 35]. Table 4 summarises a few results of fibres and composites properties. Relatively high fibre volume fraction is necessary to obtain good thickness vibration mode and non-uniform distribution of fibres can deliver low transfer of stress between matrix and ceramic fibres and non uniform strain distribution [36]. Piezo-composite performance obtained is slightly higher than that of bulk ceramic (as k_t) due to a lower acoustic impedance.

2-2 piezo-composites (Figure 10(a)), corresponding to alternative layers of piezoceramic and polymer are also developed for high frequency applications, in particular for linear arrays. For this, the thickness of each layer must be very low. To make a linear array at 30 MHz, a first fabrication process had been described [37] where polished ceramic plates (thickness around 30 μm) were bonded with epoxy resin containing polystyrene microspheres (diameter around 6 μm). To decrease the thickness, tape-casting technology and fugitive carbon ink layer has been recently developed

[38]. By a slow heating, carbon ink is eliminated, the composite is then sintered and space between ceramic layers is filled by epoxy resin under vacuum (Figure 10(b)). With these materials, linear arrays with a centre frequency over 35 MHz are conceivable.

Table 4 : Properties of 1-3 piezo-composites integrated ceramic fibre.

Fibre material	V_f (%)	ϕ (µm)	k_t (%)	$\varepsilon_{33}/\varepsilon_0$	ρ (kg/m^3)	v_l (m/s)	δ_e (%)	Q_m	T_{co}(µm)	ref
PsmT	68	35	51	120*	5480	-	-	2.95	32	[39]
PLZT	66	25	55	930*		-	-	2	35	[40]
PZT	45	17	60	201	3300	3943	0.1	100	32	[36]

V_f : fibre volume fraction; ϕ: fibre diameter; k_t: thickness coupling factor; $\varepsilon_{33}^S/\varepsilon_0$: clamped dielectric constant; ρ: density; v_l: longitudinal wave velocity; δ_e: dielectric losses; Q_m: mechanical coefficient ; T_{co}: composite thickness made ; (*measured at low frequency 1kHz)

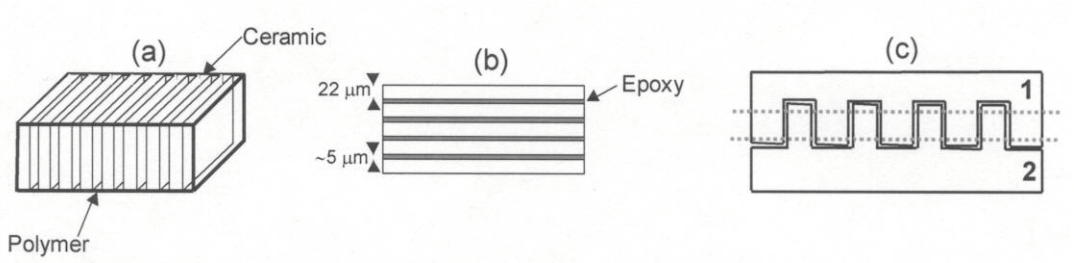

Figure 10 : (a) Schematic representation of a 2-2 piezo-composite sample. (b) Schematic cross-section of a high frequency 2-2 piezo-composites used. (c) Schematic representation of Interdigital Pair Bonding process.

Another alternative method is the Interdigital Pair Bonding [41]. This process consists in the dicing of two ceramic plates in 2-2 composites where the width of cutting grooves is slightly higher than the width of the ceramic stripe. Two 2-2 composites (parts 1 and 2 and Figure 10(c)) are obtained. One of these samples is filled with polymer and the other is inserted as described in Figure 10(c)). The final step is the curing of polymer and removal by lapping of the upper and lower parts to obtain the 2-2 composite defined between the two dashed lines (Figure 10(c)). The respective thickness for the ceramic and polymer are 36 and 4 µm [41]. The ceramic volume fraction is high. This process can be repeated in a perpendicular direction to obtain 1-3 piezo-composites.

0-3 piezo-composite, which corresponds to ceramic particles embedded in a polymer matrix (Figure 11) can also be used. Thin layers can be achieved using tape-casting or screen-printing process. Moreover, as for piezoelectric polymer, shaping is easy due to the polymer matrix. The effective properties corresponding to this connectivity are relatively poor and to obtain sufficient electromechanical performance, high ceramic volume fraction is necessary (over 60%) [42, 43]. This leads to a mixed connectivity between 0-3 and 3-3 and limits the flexibility.

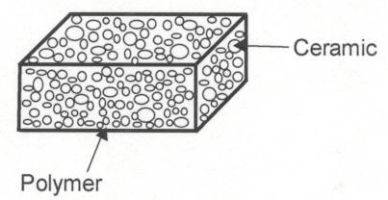

Figure 11 : Schematic representation of a 0-3 piezo-composite sample.

II.6. Hollow spheres

PT hollow spheres (few millimetre diameter) [44] are made using sacrificial polystyrene balls which are tumbled and mixed with a powder slurry. The thickness deposited can be controlled (Figure 12(1)). After calcination and sintering, the PT hollow sphere is immersed in melting wax (2) (the thickness of the melting wax allows to control the diameter of the shell) and the spheres are polished to obtain the shell (3). The thickness variations obtained are apparently low (around 10%). Finally,

the shell is removed (4), electroded and poled (5). This fabrication technique allows to obtain directly the final shape with low f-number. Properties measured on a sample from [44] are given in Table 5.

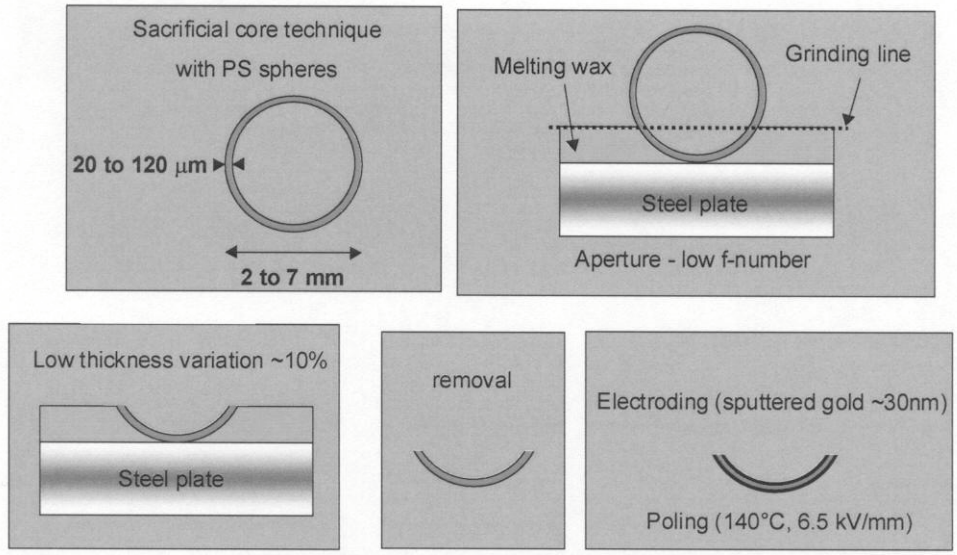

Figure 12 : Main steps for the shell fabrication based on hollow sphere.

Table 5 : Properties of shell samples.

Material - shell	$\varepsilon_{33}^T/\varepsilon_0$	f_a (MHz)	k_t (%)	d_{33} (pC/N)	δ_e (%)	δ_m (%)	**ref**
PT	280	~50	48-52	68	<2	12-17	[44]

$\varepsilon_{33}^T/\varepsilon_0$: clamped dielectric constant; f_a: antiresonant frequency; k_t: thickness coupling factor; d_{33}: piezoelectric coeffcient; δ_e: dielectric losses; δ_m: mechanical losses.

III. Transducer fabrication

III.1. Spherically shaped transducers

This fabrication technique, described by Lockwood et *al.* [45], has allowed to increase significantly the sensitivity of focused transducers, for centre frequencies around 50 MHz, compared to the more classical polymer-based devices. This method has been applied to both ceramic and single crystals (Figure 13). First, bulk ceramic is bonded on a malleable substrate (typically conductive epoxy layer) (1). Ceramic is then lapped to required thickness (generally few tens of microns) (2). The third step is the lapping of the substrate generally to around 100 microns and machining of the structure to final diameter. The two-layer composite is then heated and pressed into a spherically shaped well. The diameter of the well is the focal distance of the transducer (4). The shell is cooled and removed from the well (5). Finally, an attenuating backing is added.

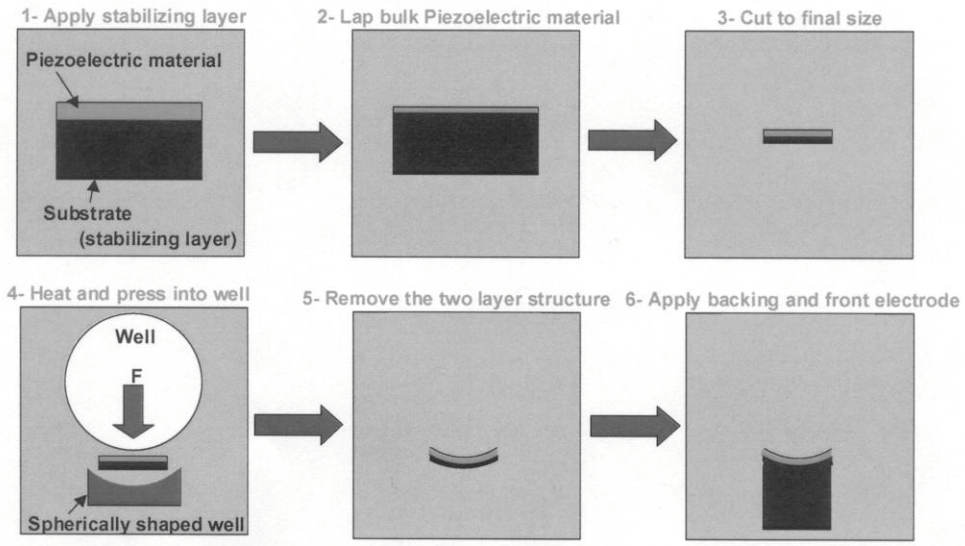

Figure 13 : Diagram describing the main steps to obtain a spherically shaped ceramic transducer.

III.2. Cross section diagrams

Two possibilities exist for focusing. The first is the use of a spherically-shaped active element (Figure 14(a)), the second is the addition of lens (Figure 14(b)). In the case of a lens, a matching layer is first deposited on the flat piezoelectric element (section I.1) and by a moulding step, the lens is added (section I.2) (Figure 14(b)). For a press-focused transducer, the addition of a curved matching layer with constant thickness is more difficult. This can be made by spin coating for loaded epoxy, or by evaporation of a Parylene^{TM} layer. Depending on the conductivity of the backing, electrical contacts are either made in this backing or on the rear face of the piezoelectric element. For the front face, the contact is made directly on the top electrode. A coaxial cable or SMA connector is finally added.

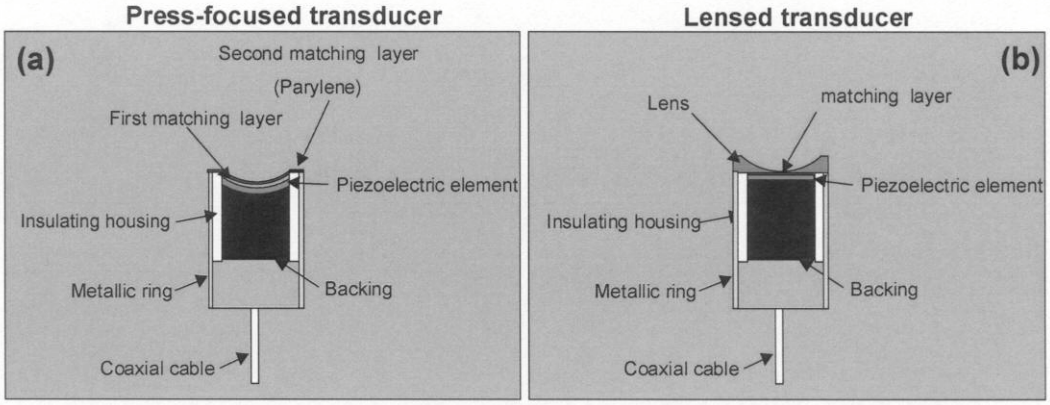

Figure 14 : Cross-sections of schematic representation of transducers (a) press-focused and (b) lens-focused.

III.3. Cable

Cables always have an influence on the electroacoustic response of a transducer but it becomes more critical at high frequencies. The choice of the cable properties (impedance, length) must be taken into account in the optimisation process [46]. On Figure 15, electroacoustic time and frequency responses of a high frequency single-element transducer (where performance has been first optimised without cable (see section IV.2)), are given for different cable lengths.

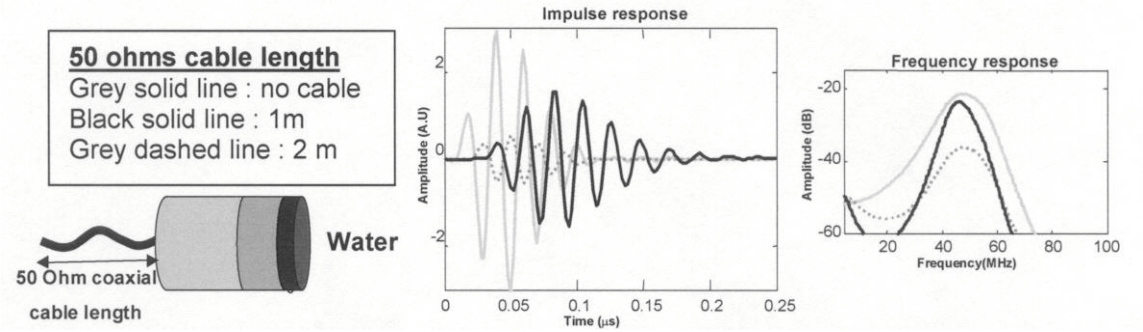

Figure 15 : (a) Schematic view of the simulated single-element transducer. (b) Electroacoustic time responses. (c) Frequency responses.

Results clearly show that the cable can affect both the sensitivity and the bandwidth.

III.4. Overview of published results

The two next Tables (Tables 6 and 7) give an overview of published results on high-frequency transducers using materials and/or process described in previous sections. Table 6 specifies essentially the characteristics (fabrication process, dimensions or material used) while Table 7 gives the corresponding performance such as bandwidth and sensitivity [28, 36, 47, 48] (if authors give these values). Concerning the sensitivity, the comparison between values is not always possible since the definition used by different authors is not identical.

Table 6 : Overview of published results on high-frequency transducers (part 1).

Material	**e** (μm)	$\mathbf{f_c}$(MHz)	shaping	$\mathbf{F_\#/F}$ (mm)	$\mathbf{Z_b}$(MRa)-material	$\mathbf{Z_{m1}}$(MRa)-material	$\mathbf{Z_{m2}}$(MRa)-material
P(VDF-TrFE) [19]	17	34	prefocused	2.7/6	15 – Ag epoxy	no	no
PVDF[36]	9	48.1	prefocused	2-3/-	3.15 –pure epoxy	no	no
$LiNbO_3$ crystal [47]	-	78	prefocused	2/-	5.9 – Ag epoxy	7.3 – Ag epoxy	2.6 - parylene
$LiNbO_3$ crystal [36]	60	44.5	lens (epoxy)	2-3/-	5.9 – Ag epoxy	7.3 – Ag epoxy	no
$LiNbO_3$ crystal [48]	-	200	prefocused	1.15/0.8	4.3 – Ag epoxy	no	no
PT ceramic [36]	32	45.1	prefocused	2-3/-	5.9 – Ag epoxy	3- parylene	no
Fiber composite [39]	32	31	prefocused	-/17.5	Porous polymer	no	no
PT hollow sphere [44]	70-90	39.8	-	-/1.43	6 - Ag epoxy	parylene	no
PZT thick film [28]	-	72	prefocused	-/2.8	Ag epoxy	no	no

e: thickness of the piezoelectric material; $\mathbf{f_c}$: transducer centre frequency; **F**: focal distance;
$\mathbf{F_\#}$: f-number; $\mathbf{Z_b}$: acoustic impedance of the backing - corresponding material;
$\mathbf{Z_{m1}}$ and $\mathbf{Z_{m2}}$: acoustic impedances of the first and second matching layers - corresponding material.

In these nine high-frequency transducers, a wide range of centre frequencies is observed (between 31 and 200 MHz). The press-focused process is essentially used. A majority of transducers have been designed to have a f-number between 2 and 3. With PT hollow sphere, this f-number is lower. For backing material, epoxy loaded with silver particles is mainly used. For matching layers, technology takes a very important place and generally only one matching layer is added. These matching layers are often in Parylene^{TM} which allows uniform and repeatable deposition of controlled-thickness layers.

Table 7 : Overview of published results of high-frequency transducers (part 2).

Material	**D** (mm)	**tuning**	**BW** (%)	**AR** (μm)	**LR** (μm)	**IL** (dB)
P(VDF-TrFE) [19]	2.2	no	70	51	-	-
PVDF [36]	3	no	118	-	-	-45.6
$LibO_3$ crystal [47]	3	yes	73	-	-	-13.5
$LiNbO_3$ crystal [36]	3	yes	74	-	-	-21.3
$LiNbO_3$ crystal [48]	0.7	-	22	12	14	-18
PT ceramic [36]	3	yes	47	-	-	-23.7
Fiber composite [39]	5	no	118	-	-	-29.3
PT hollow sphere [44]	2	no	33	-	-	-20.1
PZT thick film [28]	1	no	52	20	295	-46

D: aperture; **tuning**: addition or not of a self inductor and a transformer; **BW**: bandwidth at –6dB;
AR: axial resolution (-6dB); **LR**: lateral resolution (-6dB); **IL**: insertion loss.

In accordance with properties given in section II for piezoelectric materials, $LiNbO_3$ and PT based single-element transducers deliver best performance for medical imaging corresponding to a good trade-off between resolution and sensitivity. Press-focused process seems to deliver better performance than lens-focused process [47]. Attenuation due to various lens thickness decreases the sensitivity (around -6dB for LiNbO3 transducers [47]) even if bandwidth is slightly increased. Moreover, $LiNbO_3$ single crystal seems to be a good candidate since the lapping is not limited by grain size. Finally, the transducer ($LiNbO_3$ based) with two matching layers (Ag epoxy and parylene) gives, as expected, the highest performance.

IV. Performance

IV.1. Modelling

Electroacoustic behaviour of transducers includes electrical input impedance (that will govern energy transfer between the imaging system and the transducer), pulse-echo response (whose amplitude is linked to sensitivity and duration to axial resolution), and frequency response equal to the Fourier transform of pulse-echo response (which defines centre frequency and bandwidth). All these curves can be predicted with the assumption of single axis vibration, using equivalent electrical circuits such as KLM [10, 49] or others [50]. All transducer layers are taken into account as well as electrical elements such as electrical matching and cables. Finite element methods are also available [51, 52] in cases where no assumptions can be made on acoustic modes.

Acoustic radiation patterns allow to define lateral resolution, which is high when lateral beam dimensions are low, and acoustic noise level (the off-axis power level measured in dB using the on-axis power level as a reference). The appearance of side lobes (which exist whenever there are amplitude steps on the surface defined by the transducer front face) or grating lobes (which are due to space sampling in arrays) tends to increase acoustic noise level. Lateral resolution is responsible for image sharpness and low parasitic lobe levels ensure the absence of artefacts in the lateral direction. Radiation pattern calculations can be performed by applying Huygen's principle (*i.e.* the transducer surface is assumed to be a series of point-sources, and the pressure radiated at any point is the sum of pressures radiated by each of the point-sources [53]). For simple geometry (circular, annular or rectangular transducers), analytical results have been derived (impulse diffraction theories), and allow more efficient calculations [54, 55].

IV.2. Optimisation

Methods based on minimisation index have been developed [56, 57] in addition to analytical approaches [6, 58]. The main difficulty is first to choose the parameters and their contribution to the index. These parameters are determined as a function of the application and independently of the transducer configuration. Moreover, their calculations require only the electroacoustic response of the transducer. For medical imaging, transducers must have good resolution while keeping high sensitivity and the best trade-off must be found between these two conditions. To quantify these properties, as described on Figure 16, the three following parameters are defined: *d6*, *d30* (related to resolution) and *amp* (related to the sensitivity).

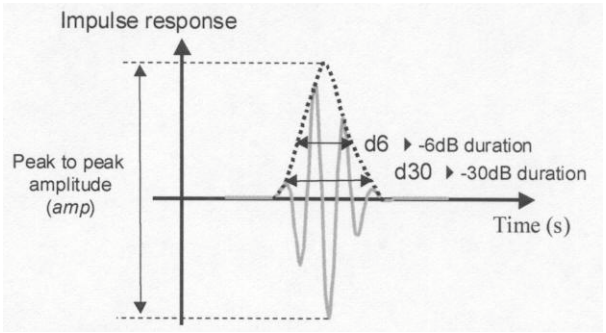

Figure 16 : Parameters used for performance index calculation from the transducer electroacoustic response.

Weighting parameters (noted α, β, γ) are applied to *d6*, *d30* and *amp*. Different trials have shown that α=8, β=8 and γ=3 lead to a performance index well adapted to medical imaging requirements:

$$PI=\alpha(d6/T_0)+\beta\ (d30/T_0)+\gamma(amp\times T_0) \quad (5)$$

T_0 is the period corresponding to the centre frequency of the transducer. Other performance indexes can be defined [56, 59]. From an initial configuration of the transducer, the electroacoustic response and then the PI are first calculated using for example the K.L.M. model. With a minimisation method such as, for example, the simplex method, transducer characteristics are modified by iteration to obtain the minimal index and the corresponding optimised configuration.

IV.3. Results & comparison

Five different piezoelectric materials have been retained for comparison. P(VDF-TrFE) copolymer, $LiNbO_3$ single crystal, lead titanate ($PbTiO_3$) ceramic, soft PZT ceramic and finally a new PMN-PT single crystal will be compared.

For all these simulations, three parameters have been fixed: the transducer centre frequency (50 MHz), the active area of the piezoelectric element (diameter of 3 mm *i.e.* an area of 7.07 mm^2) and the length of the 50 ohms coaxial cable (1.5 m). The active material thickness is adjusted to reach the 50 MHz frequency and one matching layer is considered for all these optimisations. A self inductor and a transformer are also taken into account (Figure 17). Table 8 gives all the parameters of piezoelectric materials used for the simulations (values from literature).

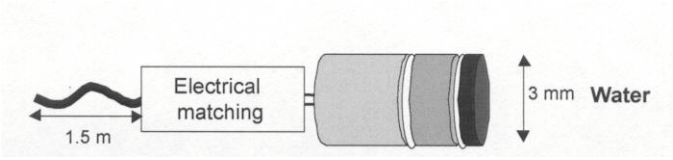

Figure 17 : Scheme of simulated transducers.

Table 8 : Piezoelectric material parameters for high-frequency single element transducer simulations.

Material	k_t (%)	$\varepsilon_{33}^S/\varepsilon_0$	ρ (kg/m^3)	v_l (m/s)	δ_e (%)	δ_m (%)	**Z** (MRa)
P(VDF-TrFE) [19]	33	4.1	1932	2380	6.9	4.0	**4.6**
$LiNbO_3$ crystal [36]	**49**	28	4640	7340	0.1	0.01	34.1
PT ceramic [36]	**49**	**200**	6900	5200	0.9	0.83	35.9
PZT soft ceramic [60]	50	800	7900	4390	2.5	2.7	34.7
PMN-33%PT [61]	**62**	712	8060	4645	-	-	37.4

k_t: thickness coupling factor; $\varepsilon_{33}^S/\varepsilon_0$: clamped dielectric constant; ρ: density;
v_l: longitudinal wave velocity; δ_e: dielectric losses; δ_m: mechanical losses; **Z**: acoustic impedance.

The optimisation of the performance of each transducer allows to determine the characteristics of the matching layer (acoustic impedance and thickness), of the backing (only its acoustic impedance since this medium is supposed semi-infinite), the value of the self inductor and the ratio of the transformer. The results are summarised in Table 9 with the values of the insertion loss (calculated as the ratio between the received power and the power delivered by the generator in pulse echo mode) and the bandwidth at –6 dB.

These simulations do not take into account the possibility of focusing by addition of lens. These results allow, for an identical configuration, to quantify the gain and compare the piezoelectric materials. Impulse responses are presented in Figure 18. Due to is relatively low k_t, the P(VDF-TrFE) based transducer delivers a relatively low sensitivity in comparison with all other simulations. The results for $PbTiO_3$ and soft PZT are similar. The electrical matching allows to compensate the differences in dielectric constants. The $LiNbO_3$ single crystal delivers a similar bandwidth but a lower sensitivity since the dielectric constant is low. Finally, the PMN-PT single crystal gives the best trade-off in terms of sensitivity and bandwidth.

Table 9 : Design and performance parameters of high-frequency single element transducers.

Material	**e** (µm)	Z_b(MRa)	Z_{m1}(MRa)	e_{m1}(×λ/4)	**tuning**	**BW**(%)	**IL**(dB)
P(VDF-TrFE)	22.4	1.2	2	1.5	Yes	71	26
$LiNbO_3$ crystal	69.6	4.5	4	1.2	Yes	70	23.4
PT ceramic	51.0	4.3	4.3	1.2	Yes	53	19.7
PZT soft ceramic	43.1	4	4.2	1.2	Yes	54	20.6
PMN-33%PT	44.3	2.7	4	1.0	Yes	**68**	**22**

e: thickness of the piezoelectric material; Z_b and Z_{m1}: acoustic impedances of the backing and matching layer;
e_{m1}: thickness of the matching layer normalised by a quarter-wavelength;
tuning: addition or not of a self inductor and a transformer; **BW**: bandwidth at –6dB; **IL**: insertion loss.

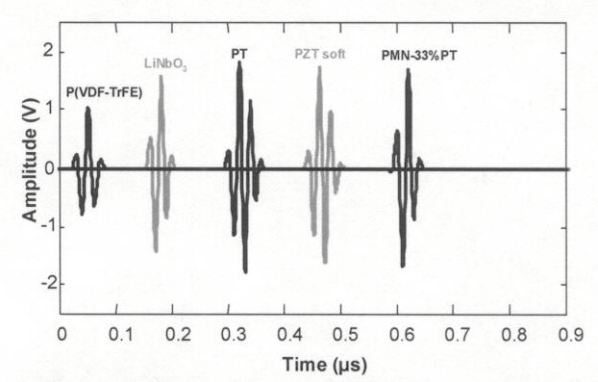

Figure 18 : Electroacoustic responses of the five simulated transducers.

V. Transducer characterisation

V.1. Passive materials

Ultrasonic spectroscopy is generally used for measurement of high frequency properties of passive materials. The method is described in [62] to measure velocity and attenuation. Experimental set-up is given in Figure 19. Particular attention must be paid to the water properties such as attenuation which can not always neglected at high frequency.

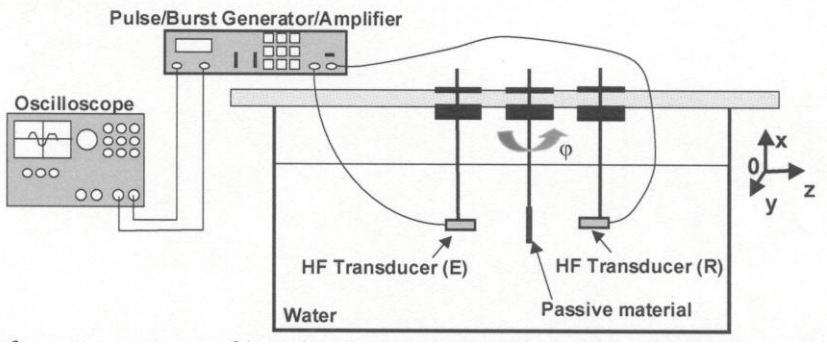

Figure 19 : Set-up of measurement of longitudinal velocity and attenuation by ultrasonic spectroscopy.

Recently, an alternative method to characterise thin passive layers was described [63]. The method is well adapted to obtain the characteristics of matching layers (thickness around 10 microns) directly at high frequency. The principle is to deposit the layer (~λ/4) on a known substrate (acoustic properties and dimensions). Then, all the signals from the thin layer are used to obtain phase velocity and attenuation (Figure 20(a)).

Another possibility is to use a resonance technique. For this, a thin piezoelectric disk (with resonance frequency over 30 MHz) is bonded to a substrate. The electromechanical and acoustic properties of the disk and substrate are previously measured. The thin passive layer is deposited on the front face of the piezoelectric disk and the modified electrical impedance is measured and fitted with KLM model to deduce the acoustic properties of the thin layer.

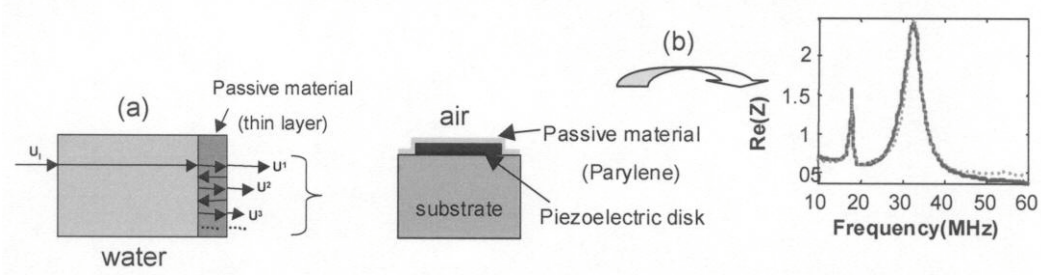

Figure 20 : (a) Experimental set-up for thin layer (~λ/4) characterisation by transmission method.
(b) Experimental set-up for thin layer characterisation by resonance method.

For these two methods, velocities are obtained with good accuracy, but not the attenuation. Velocities of a Ag epoxy or Parylene^{TM} matching layers have been measured by both methods.

V.2. Electroacoustic measurements

Electrical input impedance can be measured directly using a network or an impedance analyser, the front face of the transducer being in contact with a tissue-mimicking media or water. Typical frequency ranges are from one tenth of the resonance frequency of the piezoelectric layer to over twice this frequency.

Pulse-echo response is obtained by exciting the transducer by an electrical impulse of duration less than half a period of the active element resonance, and by measuring the echo reflected by a large acoustic mirror immersed in water. The waveform is usually digitised, which allows FFT to be used in order to derive frequency response curves. At half amplitude of the normalised envelope echo, pulse duration at –6dB corresponding axial resolution is calculated (Figure 21). If a burst is generated instead of a pulse, sensitivity can also calculated as described in Figure 21 with the amplitude ratio of the echo and the burst for a given frequency.

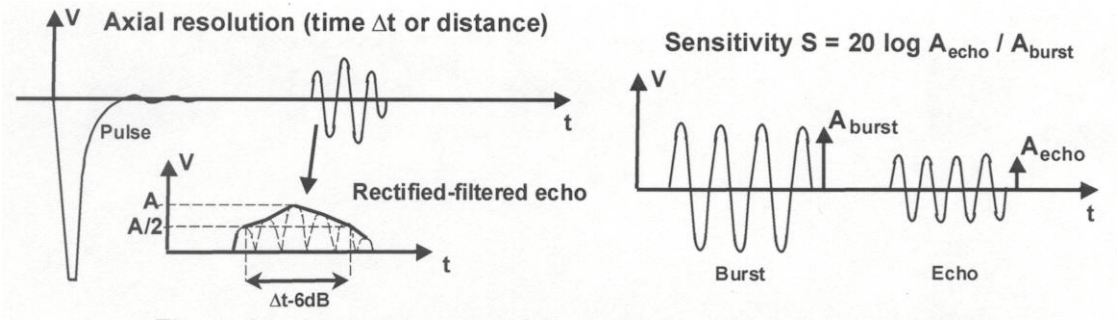

Figure 21 : Measurements of the axial resolution and sensitivity.

V.3. Radiation diagram measurements

Radiation patterns can be measured in transmit mode using a point hydrophone receiver which scan the half space in front of the transducer. Alternatively, in transmit/receive mode, a point-target is scanned, and the amplitude of the echo is plotted as function of target position. The effective diameter of the hydrophone or target must be very small: much lower than the beam width and lower than a wavelength in water. The target must not generate parasitic echoes. Lateral resolution and depth of field are measured as specified in Figure 22.

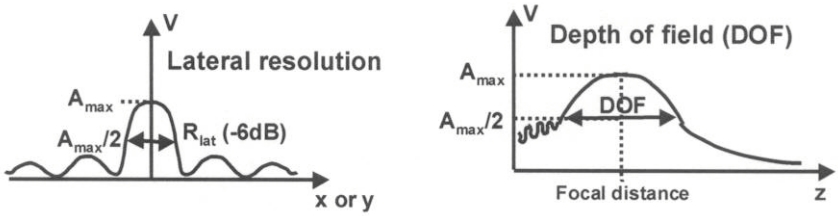

Figure 22 : Measurements of the lateral resolution and depth of field from the radiation pattern.

Specifically for high-frequency transducers, phantoms including tungsten wires (few microns diameter) with different axial and lateral spacing (typically from 500 to 30 µm) are fabricated and the images obtained when transducers are integrated in an imaging system allow to evaluate resolutions while avoiding the problem of point-target.

Interferometric laser probes can be used to measure acoustic wave displacements. With this method, excellent spatial resolution can be obtained and the high sensitivity allows to measure displacements of 10^{-3}nm/Hz$^{1/2}$ [64]. The phase variation between the reflected optical beam (on a mirror) and a reference beam corresponds to a displacement. For a focused transducer, a very thin metallised membrane can be placed perpendicularly to propagation axis (z) of the transducer. For each z value, the displacement is measured on the membrane and the radiation pattern in reconstructed [65]. Another possibility is to use the experimental set-up described in Figure 23 where optical beam and mirror are perpendicular to the axis (z) of the transducer [66]. In this case the phase variation in only due to the optical index variation induced by acoustic pressure.

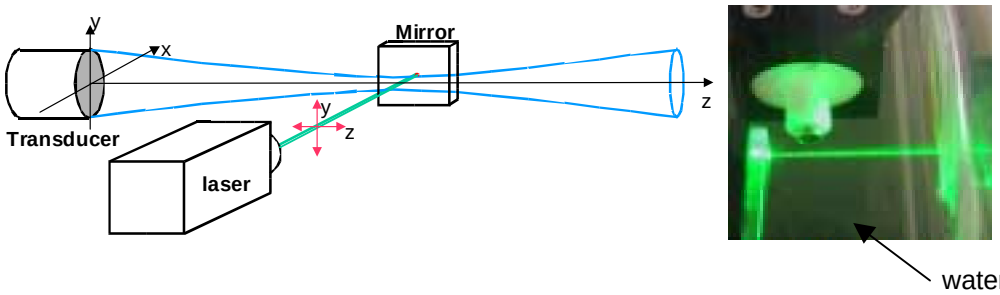

Figure 23 : Experimental set-up for acoustic pressure measurement by optical method.

This is an integral measurement, data is collected for several directions in the (x, z) plane and a tomographic reconstruction allows to obtain the pressure field. This process can be repeated at different depths to obtain the complete radiation field [67, 68].
Using this technique, measurements have been performed on a 20 MHz single element transducer. The results are given in Figure 24 [69].

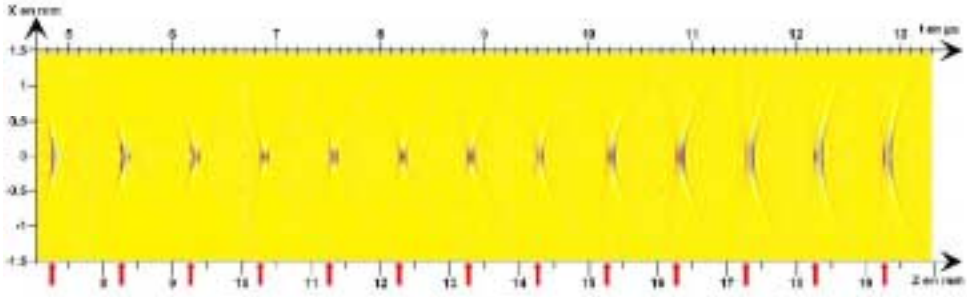

Figure 24 : Spatio-temporal evolution of acoustic beam (20 MHz transducer) between z=7 and 19mm (1mm step).

VI. Conclusion & Perspectives

High-frequency single-element transducers have been the focus of many research projects in the past years, and several technologies have been developed, some of which are industrially exploited. Polymer-based transducers have first been produced, but more recently ceramic and single crystal-based devices have proven to deliver higher performance. The trend is now moving towards array transducers [37, 70], following first attempts in the early 90's [71] around 20 MHZ. The aim is now to produce linear arrays in the 25 to 50 MHz range. Some authors are investigating high-frequency 2D arrays [72], as well as new technologies such as optical arrays [73] and capacitive micro-machined devices [74].

Acknowlegement

The authors would like to thank co-workers of LUSSI/GIP ULTRASONS in Tours & Blois and colleagues from teams involved in HF ultrasound around the world for fruitful discussions and co-operation.

References

1. Sherar, M.D., M. B. Noss, F. S. Foster, *Ultrasound backscatter microscopy images the internal structure of living tumour spheroids.* Nature, 1987. **330**: p. 493-495.
2. Berson, M., J. M. Grégoire, F. Gens, J. Rateau, F. Jamet, L. Vaillant, F. Tranquart, L. Pourcelot, *High frequency (20 MHz) ultrasonic devices: advantages and applications.* European Journal of ultrasound, 1999. **10**: p. 53-63.
3. Ermet, H., M. Vogt. *High frequency ultrasonic imaging and its applications in skin*. in *SPIE Conference on Ultrasonic Transducer Engineering*. 1999.
4. Foster, F.S., C. J. Pavlin, K. A. Harasiewicz, D. A. Christopher, D. H. Turnbull, *Advances in ultrasound biomicroscopy.* Ultrasound in Med. & biol., 2000. **26**(1): p. 1-27.
5. Kossof, G., *The effects of backing and matching on the performance of piezoelectric ceramic transducers.* IEEE Trans. Sonics and Ultrasonics, 1966. **13**: p. 20-30.
6. Desilets, C.S., J. D. Fraser, G. S. Kino, *The design of efficient broadband piezoelectric transducers.* Ultrasonics, 1978. **25**: p. 115-125.
7. Inoue, T., M. Ohta, S. Takahashi, *Design of ultrasonic transducers with multiple acoustic matching layers for medical application.* IEEE Trans. Ultrason. Ferroelect., Freq. Contr, 1987. **34**: p. 8-16.
8. Lethiecq, M., F. Levassort, G. Feuillard, L. P. Tran-Huu-Hue, *Piezoelectric materials for ultrasonic medical diagnostics.* Piezoelectric Materials in Devices, Ed. N. setter, 2002. **Chaper 11**: p. 211-230.
9. IEEE, *Standard on Piezoelectricity ANSI/IEEE Std.* 1987.
10. Krimholtz, R., D. A. Leedom, G. L. Matthei, *New equivalent circuit for elementary piezoelectric transducers.* Electronic letters, 1970. **38**: p. 338-339.
11. CENELEC, *European Standard P25EN 50324.*
12. Tran-Huu-Hue, L.P., F. Levassort, F. Vander Meulen, J. Holc, M. Kosec, M. Lethiecq, *Preparation and electromechanical properties of PZT/PGO thick films on alumina substrate.* Journal of the European Ceramic Society, 2001. **21**(10-11): p. 1445-1449.

13. Lukacs, M., T. Olding, M. Sayer, *Thickness mode material constants of a supported piezoelectric film.* Journal of Applied Physics, 1999. **85**(5): p. 2835-2843.
14. Foster, F.S., L. K. Ryan, D. H. Turnbull, *Characterization of lead zirconate titanate for use in miniature high-frequency (20-80 MHz) transducers.* IEEE Trans. Ultrason., Ferroelect., Freq. Contr., 1991. **38**: p. 1371-1376.
15. Zipparo, M. J., K. K. Shung, T. R. Shrout, *Piezoceramics for high frequency (20 to 100 MHz) single-element imaging transducers.* IEEE Trans. Ultrason., Ferroelect., Freq. Contr., 1997. **44**: p. 1038-1048.
16. Tran-Huu-Hue, L.P., F. Levassort, N. Felix, D. Damjanovic, W. Wolny, M. Lethiecq, *Comparison of several methods to characterize the high frequency behavior of piezoelectric ceramics for transducer applications.* Ultrasonics, 2000. **38**(1-8): p. 219-223.
17. Kawaii, H., *The piezoelectricity of poly(vinylidene fluoride).* Jpn. J. Appl. Phys., 1969. **8**: p. 975-976.
18. Foster, F.S., K. A. Harasiewicz, M. D. Sherar, *A history of medical and biological imaging with polyvinylidene fluoride (PVDF) transducers.* IEEE Trans. Ultrason., Ferroelect., Freq. Contr., 2000. **47**(6): p. 1363-1371.
19. Levassort, F., L. P. Tran-Huu-Hue, G. Feuillard, M. Lethiecq, *Characterisation of P(VDF-TrFE) material taking into account dielectric relaxation: application to modelling of high frequency transducers.* Ultrasonics, 1998. **36**(1-5): p. 41-45.
20. Wolny, W.W., *Piezoceramic thick films - Technology and applications. State of art in Europe.* IEEE Int. Symp. Applic. Ferro., 2001: p. 257-262.
21. Gentry, K.L., J. M. Zara, S. Bu, C. Eom, S. W. Smith, *Thick film sol PZT Transducer using dip coating.* IEEE Int. Ultrasonics Symp., 2000. **2**: p. 977-980.
22. He, X.-Y., A.-L Ding, X.-S. Zheng, P.-S. Qiu, W.-G. Luo, *Preparation of PZT(53/47) thick films deposited by a dip-coating process.* Microelectronic Engineering, 2003. **66**: p. 865-871.
23. Kobayashi, M., T. R. Olding, L. Zou, M. Sayer, C. K. Jen, A. U. Rehman, *Piezoelectric thick film ultrasonic transducers fabricated by spray technique.* IEEE Int. Ultrasonics Symp., 2000. **2**: p. 985-989.
24. Thiele, E.S., D. Damjanovic, N. Setter, *Processing and properties of screen-printed lead zirconate titanate piezoelectric thick films on electroded silicon.* J. Am. Ceram. Soc., 2000. **84**(12).
25. Levassort, F., L. P. Tran-Huu-Hue, M. Lethiecq, T. Bove, W. W. Wolny, *New piezoceramics films for high resolution medical imaging applications.* IEEE Int. Ultrasonics Symp., 2000. **2**(6): p. 1125-1128.
26. Thiele, E.S., N. Setter, *Lead zirconate titanate particle dispersion in thick-film ink formulations.* J. Am. Ceram. Soc., 2000. **83**(6).
27. Kosec, M., J. Holc, F. Levassort, L. P. Tran-Huu-Hue, M. Lethiecq, *Screen-printed Pb(Zr,Ti)O3 thick films for ultrasonic medical imaging applications.* Proc. 34th Int. Symp. on Microelectronics, 2001: p. 195-200.
28. Lukacs, M., M. Sayer, F. S. Foster, *Single element high frequency (>50 MHz) PZT sol gel composite ultrasound transducers.* IEEE Trans. Ultrason., Ferroelect., Freq. Contr., 2000. **47**(1): p. 148-159.
29. Newnham, R.E., D. P. Skinner, L. E. Cross, *Connectivity and piezoelectric-pyroelectric composites.* Mat. Res. Bull., 1978. **13**: p. 525-536.
30. Savakus, H. P., K. A. Klicker, R. E. Newnham, *PZT-Epoxy piezoelectric transducers: a simpliflied fabrication procedure.* Mat. Res. Bull., 1981. **16**: p. 677-680.
31. Janas, V. F., A. Safari, *Overview of fine-scale piezoelectric ceramic/polymer composite processing.* 1995. **78**(11): p. 2945-2955.
32. Su, B., D. H. Pearce, T. W. Button, *Routes to net shape electroceramic devices and thick films.* J. Eur. Ceram. Soc., 2001. **21**: p. 2005-2009.
33. Meyer Jr, R.J., P. Lopath, S. Yoshikawa, T. R. shrout, *High frequency 1-3 composite transducers fabricated from alkoxide-derived PZT fibers.* IEEE Int. Ultrasonics Symp., 1997: p. 915-918.
34. Jadidian, B., V. Janas, A. safari, J. French, G. Weitz, J. Luke, R. Cass, *Development of fine scale piezoelectric ceramic/polymer composites via incorporation of fine PZT fibers.* IEEE Int. Ultrasonics Symp., 1996: p. 31-34.
35. Meyer Jr, R.J., T. R. Shrout, S. Yoshikawa, *Development of ultra-fine scale piezoelectric fibers for use in high frequency 1-3 transducers.* IEEE Int. Ultrasonics Symp., 1996: p. 547-550.
36. Snook, K. A., J.-Z Zhao, C. H. F. Alves, J. M. Cannata, W.-H. Chen, R. J. Meyer, T. A. Ritter, K. K. Shung, *Design, Fabrication, and evaluation of high frequency, single-element transducers incorporating different materials.* IEEE Trans. Ultrason., Ferroelect., Freq. Contr., 2002. **49**(2): p. 169-176.
37. Ritter, T.A., T. R. Shrout, R. Tutwiler, K. K. Shung, *A 30-MHz piezo-composite ultrasound array for medical applications.* IEEE Trans. Ultrason., Ferroelect., Freq. Contr., 2002. **49**(2): p. 217-230.
38. Kwon, S., W. Hachenberger, P. Rehrig, K. Snook, S. Rhee, T. R. Shrout, *Ceramic/polymer 2-2 composites for high frequency transducers by Tape-casting.* IEEE Int. Ultrasonics Symp., 2003: p. 366-369.
39. Li, K., H. L. W. Chan, C. L. Choy, *Samarium and manganese-doped lead titanate ceramic fiber/epoxy 1-3 composite for high-frequency transducer application.* IEEE Trans. Ultrason., Ferroelect., Freq. Contr., 2003. **50**(10): p. 1371-1376.
40. Chan, H.L.-W., K. Li, C.-L Choy, *Piezoelectric ceramic fibre/epoxy 1-3 composites for high-frequency ultrasonic transducer applications.* Materials Science and Engineering B, 2003. **99**: p. 29-35.
41. Liu, R., D. knapik, K. A. Harasiewicz, F. S. Foster, *Fabrication of 2-2 Piezoelectric composites by Interdigital Pair Bonding.* IEEE Int. Ultrasonics Symp., 1999: p. 973-976.
42. Levassort, F., M. Lethiecq, D. Certon, F. Patat, *A matrix method for modeling electroelastic moduli of 0-3 piezo-composites.* IEEE Trans. Ultrason. Ferroelect., Freq. Contr, 1997. **44**(2): p. 445-452.
43. Levassort, F., M. Lethiecq, R. Desmare, L. P. Tran-Huu-Hue, *Effective electroelastic moduli of 3-3(0-3) piezocomposites.* IEEE Trans. Ultrason. Ferroelect., Freq. Contr, 1999. **46**(4): p. 1028-1034.

44. Meyer Jr, R.J., R. E. Newnham, S. Alkoy, T. Ritter, J. Cochran Jr, *Pre-focused lead titanate >25 MHz single-element transducers from hollow spheres.* IEEE Trans. Ultrason., Ferroelect., Freq. Contr., 2001. **48**(2): p. 488.
45. Lockwood, G.R., D. H. Turnbull, F. S. Foster, *Fabrication of spherically shaped ceramic transducers.* IEEE Trans. Ultrason., Ferroelect., Freq. Contr., 1994. **41**(2): p. 231-235.
46. Chen, W. H., P. J. Cao, E. Maione, T. Ritter, K. K. shung, *Optimization of pulse transmission in a high frequency ultrasound imaging system.* IEEE Int. Ultrasonics Symp., 2001: p. 995-998.
47. Cannata, J.M., T. A. Ritter, W.-C. Chen, R. H. Silverman, K. K. Shung, *Design of efficient, broadband single-element (20-80 MHz) ultrasonic transducers for medical imaging applications.* IEEE Trans. Ultrason., Ferroelect., Freq. Contr., 2003. **50**(11): p. 1548-1557.
48. Knapik, D. A., B. Starkoski, C. J. Pavlin, F. S. Foster, *A 100-200 MHz ultrasound biomicroscope.* IEEE Trans. Ultrason., Ferroelect., Freq. Contr., 2000. **47**(6): p. 1540-1549.
49. Van Kervel, S. J. H., J. M. Thijssen, *A calculation scheme for the optimum design of ultrasonic transducers.* Ultrasonics, 1983. **21**: p. 134-140.
50. Lockwood, G. R., F. S. Foster, *Modeling and optimization of high-frequency ultrasound transducers.* IEEE Trans. Ultrason., Ferroelect., Freq. Contr., 1994. **41**(2): p. 225-230.
51. Assaad, J., B. Dubus, B. Hamonic, J. N. Decarpigny, J. C. Debus, *Finite element modelling of ultrasonic transducers using the ATILA code.* Proceedings of Ultrasonics International, 1991: p. 371-374.
52. Marechal, P., F. Levassort, L. P. Tran-Huu-Hue, M. Lethiecq, *Electro-acoustic response at the focal point of a focused transducer as a function of the acoustical properties of the lens.* Proc. 5th World Congress on Ultrasonics, 2003: p. 535-538.
53. Kino, G.S., *Acoustic waves: devices imaging and analog signal processing*. 1987: processing Prentice-Hall Inc Englewood Cliffs New Jersey. Chap. 3.
54. Penttinen, A., M. Luukkala, *The impulse response and pressure nearfield of a curved ultrasonics radiators.* J. Phys. D, 1976. **9**: p. 1547-1557.
55. Selfridge, A.R., G. S. Kino, B. T. Khury-Yakub, *A theory for the radiation pattern of a narrow strip acoustic transducer.* Appl. Phys. Lett., 1980. **37**: p. 35-36.
56. Thijssen, J. M., W. A. Verhoef, M. J. Cloostermans, *Optimisation of ultrasonic transducers.* Ultrasonics, 1985: p. 41-46.
57. Rhyne, T. L., *Computer optimisation of transducer transfer using constraints on bandwidth, ripple and loss.* IEEE Trans. Ultrason., Ferroelect., Freq. Contr., 1996. **43**(6): p. 1136-1149.
58. Mc Keighen, R. E., *Design guidelines for medical ultrasonic arrays.* S.P.I.E., 1998. **3341**: p. 2-18.
59. Desmare, R., L. P. Tran-Huu-Hue, F. Levassort, M. Lethiecq, *Optimisation method for ultrasonic transducers used in medical imaging.* Journal Revista de Acustica, 2003. **33**.
60. Felix, N., L. P. Tran-Huu-Hue, L. Walker, C. Millar, M. Lethiecq, *The application of high permittivity piezoelectric ceramics to 2D array transducers for medical imaging.* Ultrasonics, 2000. **38**: p. 127-130.
61. Zhang, R., B. Jiang, W. Cao, *Orientation dependence of piezoelectric properties of single domain 0.67Pb(Mn1/3Nb2/3)03-0.33PbTiO3 crystals.* Appl. Phys. Lett., 2003. **82**(21): p. 3737-3739.
62. Wang, H., T. Ritter, W. Cao, K. K. Shung, *High frequency properties of passive materials for ultrasonic transducers.* IEEE Trans. Ultrason., Ferroelect., Freq. Contr., 2001. **48**(1): p. 78-84.
63. Wang, H., W. Cao, *Characterizing ultra-thin matching layers of high-frequency ultrasonic transducer based on impedance matching principle.* IEEE Trans. Ultrason., Ferroelect., Freq. Contr., 2004. **51**(2).
64. Royer, D., E. Dieulesaint, *Mesures optiques de déplacement d'amplitude 10^{-4} à 10^{2} Angström. Application aux ondes élastiques.* Rev. Phys. Appl., 1989: p. 833-846.
65. Royer, D., O. Casula, *Quantitative imaging of transient acoustic fields by optical heterodyne interferometry.* IEEE Int. Ultrasonics Symp., 1994: p. 1153-1162.
66. Jia, X., G. Quentin, M. Lassoued, *Optical heterodyne detection of pulsed ultrasonic pressures.* IEEE Trans. Ultrason., Ferroelect., Freq. Contr., 1993. **43**(1): p. 67-69.
67. Bou Matar, O., L. Pizarro, D. Certon, J. P. Remenieras, F. Patat, *Characterization of airborne transducers by optical tomography.* Ultrasonics, 2000. **38**: p. 787-793.
68. Remenieras, J.-P., O. BouMatar, S. Callé, F. Patat, *Acoustic pressure measurement by acousto-optic tomography.* IEEE Int. Ultrasonics Symp., 1991.
69. Grégoire, J.M., *Echographie haute-résolution : technologie et applications en dermatologie et ophtalmologie.* Ph.D Thesis (in French) University François Rabelais, Tours, 2002.
70. Lacaze, E., S. Michau, P. Mauchamp, *20 MHz ultrasound array for medical imaging: from design to image evaluation.* IEEE Int. Ultrasonics Symp., 2001: p. 1139-1142.
71. Lethiecq, M., G. Feuillard, L. Ratsimandresey, A. Nguyen-Dinh, L. Pardo, J. Ricote, B. Andersen, C. Millar, *Miniature high frequency array transducers based on new fine grain ceramics.* IEEE Int. Ultrasonics Symp., 1994. **2**: p. 1009-1013.
72. Buma, T., M. Spisar, M. O'Donnell, *A high-frequency, 2D array element using thermoelastic expansion in PDMS.* IEEE Trans. Ultrason., Ferroelect., Freq. Contr., 2003. **50**(9): p. 1161-1176.
73. Hamilton, J. D., M. O'Donnell, *High frequency ultrasound imaging with optical array.* IEEE Trans. Ultrason., Ferroelect., Freq. Contr., 1998. **45**(1): p. 216-235.
74. Oralkan, O., A. S. Ergun, J. A. Johnson, U. Demirci, M. Karaman, K. Kaviani, T. H. Lee, B. T. Khuri-Yakub, *Capacitive micromachined ultrasonic transducers: Next-generation arrays for acoustic imaging?.* IEEE Trans. Ultrason., Ferroelect., Freq. Contr., 2002. **49**(11): p. 1596-1610